Fractional Differentiation-based Hybrid Active Contour Model for Noisy Image Segmentation

Srikanth Khanna[1] and Venkatachalam Chandrasekaran[2]

[1]Assistant Professor
[2]Professor
[1,2]Department of Mathematics and Computer Science,
Sri Sathya Sai Institute of Higher Learning, Puttaparthi, Andhra Pradesh, India.
[1]srikanthkhanna@sssihl.edu.in
[2]vchandrasekaran@sssihl.edu.in

Abstract - *Image segmentation in the presence of noise is a challenging task. Performance of the methods which are efficient in noiseless images degrades in the presence of noise. In this paper, we propose a novel fractional derivative-based hybrid active contour for robust noisy image segmentation. By incorporating a novel fractional derivative-based balloon term and a fractional derivative-based edge term along with a region scalable fitting function, we obtain a method which provides good segmentation performance even in high noise scenarios without any change in the method parameters. We demonstrate that the proposed method outperforms the conventional methods in the presence of Gaussian, speckle and bipolar noises.*

Keywords - active contour, fractional derivative, level set, noisy image segmentation

I. INTRODUCTION

Image segmentation is an important step in the image processing chain. In the segmentation process, distinct constituent regions of an image are identified based on a chosen criterion. The accuracy of higher level vision processes depends on the quality of segmentation.

Over the years, several segmentation techniques have been proposed in the literature. The active contour model initiated by Kass *et al.* [1] is one of the chief segmentation techniques. These active contour methods can achieve sub-pixel level accuracy in segmentation. In an active contour model, an initial contour is introduced which is then iteratively evolved to attach to object boundary. The energy formulation captures the criterion of segmentation in this case. A higher dimensional level set [2] is generally used to represent the active contour where the zeroth level set denotes the evolving contour. The aim of the level set evolution is to obtain the actual object boundaries as the zeroth level set. The inside and outside regions thereby will be the positive and negative level sets respectively.

Active contour methods use a variety of energy concepts to accurately segment the images. There are two chief types of active contour models - edge-based models [3], [4], [5], [6] and region-based models [7], [8], [9], [10], [11], [12]. In both these types image statistics are used for effective segmentation. The edge-based models use the image gradient response in an edge detector to evolve the contour to the desired object boundaries. These models are therefore sensitive to noise and may not be efficient in scenarios where the gradient is weak. The region-based models, on the other hand, endeavor to capture the region description using statistics. The region-based models are effective even in scenarios, where the gradient information is unavailable [8]. The weakness of region-based active contour models is that they tend to characterize the object using a statistical model, which may not hold in every real world setting. Hence, research into hybrid approaches is also available in the literature, which combine global and local information for accurate segmentation [13], [14].

In this work, we propose a new hybrid active contour method for the segmentation of noisy images. For robust performance in the presence of high noise, we use two fractional derivative-based terms - a novel fractional derivative-based bidirectional balloon term and an edge term - in the evolution criterion, alongside the region scalable fitting term as in [11]. As demonstrated in the following sections, the proposed hybrid model outperforms the individual constituents and provides a better segmentation method in combination.

II. BACKGROUND AND RELATED METHODS

A. *Fractional Differentiation Preliminaries*

Fractional derivatives, which are a generalization of integer order derivatives, have been found to be superior in modelling long memory effects. There are many definitions given for the general order derivatives. In this work, we use the Grunwald-Letnikov(G-L) definition owing to its series definition and ease of implementation. We use the one dimensional G-L fractional derivative definition to obtain the one-sided fractional image derivatives on either side of the evolving active contour. Here we give the definitions. Let $\theta(x, y)$ be the direction of gradient of the contour $\phi(x, y)$ computed at a location (x, y) in the level set formulation. If $I(x, y)$ denotes the image, α-th order one-sided fractional derivatives can be computed as follows:

$$D_\theta^\alpha I(x, y) = h^{-\alpha} \sum_{j=0}^{N_1} (-1)^j \binom{\alpha}{j} I(x + \tau_1, y + \tau_2) \quad (1)$$

and

$$D_{\theta+180}^\alpha I(x, y) = h^{-\alpha} \sum_{j=0}^{N_2} (-1)^j \binom{\alpha}{j} I(x - \tau_1, y - \tau_2) \quad (2)$$

where $\tau_1 = jhcos\theta$ and $\tau_2 = jhsin\theta$. As can be seen from the definitions, these fractional derivatives bring in additional region information when compared to the integer order derivatives, and when moulded as an edge-based energy, can assist in efficient delineation of object boundaries.

B. Related Active Contour Models

The use of fractional derivatives in image segmentation is mainly through the use in active contour framework. The data fitting term and a length penalty term are a common feature of region-based active contour models. The fractional derivative-based improvement is through either of these terms or an edge indicator function.

In [15], a two stage model is proposed. In the first, morphological gradient was used to extract the transition region and in the second a fractional order edge indicator-based external energy was used in the geometric active contour model. By incorporating the fractional derivative-based term in the length term, the noise influence was mitigated. In [16], a fractional-order diffusion-based edge indicator is employed to counter the effect of intensity inhomogeneity. The fuzzy signed pressure force and fuzzy local fitting alongside the fractional derivative term make the method robust and accurate. In [17], unlike the regular gradient-based energy minimization, a fractional derivative of Mittag-Leffler-based energy minimization is employed. The new technique maintains the high frequency content while enhancing texture detail. This is applied on kidney MRI image segmentation. In [18], the authors use fractional calculus to overcome the shortcomings of the distance regularized level

set function. The fractional distance regularization term penalizes any deviation from the signed distance function. G-L definition-based conjugate of fractional derivatives and the fractional divergence term were derived. The method was demonstrated to be performing better with weak images and intensity inhomogeneity. In [19], local fractional derivative-based fitting energy is defined to counter the effect of intensity inhomogeneity. Eight fractional derivative masks proposed by Tian *et al.* were used for this purpose. In [20], the fractional order fitting term is obtained by the frequency domain implementation. The level set evolution was demonstrated to be robust and stable. In [21], fractional order gradient magnitude is obtained in the first step using frequency domain implementation. A difference of this magnitude with the original image is computed and used for local fitting energy term. A weighted combination of global and local fitting terms with a length penalty drives the level set evolution. The weight of global vs local fitting is decided adaptively using the local contrast ratio of the gradient image. The method was shown to effective in inhomogeneous image segmentation.

Now we discuss in detail the methods which are related to the proposed model. Firstly, we briefly present the Chan-Vese model and then describe the region scalable fitting-based models.

1) *Chan-Vese Active Contour Model*:

The Chan-Vese model is based on the piece-wise constant Mumford-Shah model. The image intensity is assumed to be homogeneous. If $I(x, y) : \Omega \to \mathcal{R}$ denotes the original image, the Chan-Vese fitting energy is given as:

$$E_{CV} = \lambda_1 \int_{inside(C)} (I - c_1)^2 dxdy + \lambda_2 \int_{outside(C)} (I - c_2)^2 dxdy \quad (3)$$

Here, c_1 and c_2 represent the mean intensity values inside and outside the evolving contour. Parameters λ_1 and λ_2 can be used to balance the weight given to inside versus outside region. Using the level set formulation the overall energy becomes

$$E_{CV} = \lambda_1 \int (I - c_1)^2 H(\phi) dxdy + \lambda_2 \int (I - c_2)^2 (1 - H(\phi)) dxdy$$
$$+ \nu \int |\nabla H(\phi)| dxdy \quad (4)$$

Here the Heaviside function $H_\epsilon(\phi)$ which denotes the interior of the contour is given as:

$$H_\epsilon(\phi) = \frac{1}{2} + \frac{1}{\pi} arctan(\frac{\phi}{\epsilon})$$

The Dirac delta, δ_ϵ, which is the derivative of $H_\epsilon(\phi)$

$$\delta_\epsilon(\phi) = \frac{\epsilon}{\pi(\phi^2 + \epsilon^2)}$$

denotes the area around the evolving contour. The parameter ϵ controls the spread of the function.

Minimizing the Eqn. 4 w.r.t. c_1 and c_2 gives the following expressions for their optimal values in the iterations:

$$c_1 = \frac{\int I(x,y)H(\phi)dxdy}{\int H(\phi)dxdy} \qquad (5)$$

$$c_2 = \frac{\int I(x,y)(1-H(\phi))dxdy}{\int (1-H(\phi))dxdy} \qquad (6)$$

These mean values c_1 and c_2 play an important role in the segmentation procedure. However, if the homogeneity assumption, inherent in the piece-wise constant model, does not hold, these values may fail to represent the region and hence, may lead to unsatisfactory segmentation.

2) *Region Scalable Fitting Active Contour Model*:

The region scalable fitting (RSF) model [11] attempts to solve the inhomogeneity problem by using data fitting values, which approximate the intensities in a limited region around the contour pixel in consideration. The size of this region is controlled by setting the appropriate scale parameter for the kernel K used in the energy formulation. The RSF energy is given by the following equation:

$$E_{RSF} = \sum_{i=1}^{2} \lambda_i \int K(x-y)(I(y)-f_i(x))^2 M_i(\phi)dy + \nu|\nabla H(\phi)|$$

The kernel K used in this formulation is a non-negative function $K : \mathcal{R}^n \to [0, +\inf)$ with the following properties:

1. $K(-u) = K(u)$

2. $K(u) \geq K(v)$, if $|u| < |v|$ and $\lim_{|u| \longrightarrow \infty} K(u) = 0$

3. $\int K(x)dx = 1$

K was chosen to be the Gaussian kernel.

$$K_\sigma(u) = \frac{1}{(\sqrt{2\pi})\sigma}e^{\frac{-|u|^2}{2\sigma^2}}$$

The energy minimization leads to the evolution equation

$$\frac{\partial\phi}{\partial t} = -\delta_\epsilon(\phi)(\lambda_1 e_1 - \lambda_2 e_2) + \nu\delta_\epsilon(\phi)div(\frac{\nabla\phi}{|\nabla\phi|})$$
$$+ \mu(\nabla^2\phi - div(\frac{\nabla\phi}{|\nabla\phi|})) \qquad (7)$$

where δ_ϵ is the regularized Dirac delta function and e_1, e_2 are given by

$$e_i(x) = \int K_\sigma(y-x)|I(x) - f_i(x)|^2 dy, i = 1, 2$$

Here f_1 and f_2 are the fitting terms which are as follows:

$$f_1(x) = \frac{K_\sigma(x) * [H_\epsilon(\phi)I(x)]}{K_\sigma(x) * H_\epsilon(\phi)} \qquad (8)$$

$$f_2(x) = \frac{K_\sigma(x) * [(1 - H_\epsilon(\phi))I(x)]}{K_\sigma(x) * (1 - H_\epsilon(\phi))} \qquad (9)$$

Comparing Eqns. (5, 6) to Eqns. (8, 9), it is evident that the region scalable fitting can be customized in size using the scale parameter as opposed to the global fitting of data in the piece-wise constant Chan-Vese model.

3) *Adaptive Fractional Order Differentiation-based Active Contour Model(AFACM)*:

In [27], Meng Li *et al.* proposed an active contour model on the lines of RSF model which deals effectively with the noise challenge in segmentation. The model has a fitting, length penalty and level set regularization components. The evolution equation of this model is as follows:

Case 1:

$$\frac{\partial\phi}{\partial t} = -\delta(\phi)[\lambda\int_\Omega K_\sigma.(I - \frac{f_1+f_2}{2})dy$$
$$+ \beta\int_\Omega K_\sigma.(D^\nu I - \frac{d_1+d_2}{2})dy + \gamma g.div(\frac{\nabla\phi}{|\nabla\phi|})]$$
$$+ \mu(\nabla^2\phi - div(\frac{\nabla\phi}{|\nabla\phi|})) \qquad (10)$$

Case 2:

$$\frac{\partial\phi}{\partial t} = -\delta(\phi)[\lambda\int_\Omega K_\sigma.(I - \frac{f_1+f_2}{2})dy$$
$$+ \beta\int_\Omega (D^\nu I - \frac{d_1+d_2}{2})dy + \gamma g.div(\frac{\nabla\phi}{|\nabla\phi|})]$$
$$+ \mu(\nabla^2\phi - div(\frac{\nabla\phi}{|\nabla\phi|})) \qquad (11)$$

As can be seen from Eqn.10 and Eqn.11, the fitting term in this model comprises of the region scalability term and the fractional derivative-based terms. f_1, f_2 are computed in the same way as in Eqn.8 and Eqn.9.

$$d_1(x) = \frac{K_\sigma(x) * [H_\epsilon(\phi)D^\nu I(x)]}{K_\sigma(x) * H_\epsilon(\phi)} \qquad (12)$$

$$d_2(x) = \frac{K_\sigma(x) * [(1 - H_\epsilon(\phi))D^\nu I(x)]}{K_\sigma(x) * (1 - H_\epsilon(\phi))} \qquad (13)$$

The fractional derivative order here is obtained adaptively using the following equation:

$$\nu(x,y) = \frac{|\nabla I(x,y)|}{\max_{(x,y)\in\Omega}|\nabla I(x,y)|} \qquad (14)$$

where $|\nabla I(x,y)| = \sqrt{((\nabla_x I(x,y))^2 + (\nabla_y I(x,y))^2)^2}$.

The authors use the degraded Chan-Vese model to further bring down the computational complexity and arrive at the evolution equations. The authors compare the two cases obtained and report that the Case-1, which has the K_σ convolution involved, is having better performance. We use this Case 1 expression later on for our comparison. This model is claimed to have got better noise insensitivity and accurate segmentation capabilities.

III. PROPOSED HYBRID METHOD

Now we discuss the formulation of the proposed active contour model. We discuss the fractional derivative terms first and then provide the evolution equation for the hybrid model.

A. Fractional Derivative-based Terms

Our active contour model is unique in the sense that the evolution is based on the fractional derivative responses in the normal direction along the evolving contour. This gives robustness in noisy scenarios and also in cases of objects with weak boundary information. We utilize this property of fractional derivatives by incorporating them into a bidirectional balloon term as well as an edge term as discussed below.

1) Edge Term:

In [22], the authors had proposed an edge term for robust noisy image segmentation. The authors had incorporated the fractional derivative difference as weight into the length regularization term of the active contour model. In the energy minimization iterations, this makes the evolving contour to actively reach out and hold on effectively to the edges as it shrinks in length. Since it is a length minimization term, it becomes necessary that the initialization envelops the target object. This model was shown to be robust to noise, however, the evolution in this case was much slower than the state-of-the art region-based terms.

The energy of this model is given as follows:

$$E_{EDGE}(\phi) = \int_{\Omega} g\delta(\phi)|\nabla\phi| \qquad (15)$$

where $g(x, y) = -(\lambda_1 D_\theta^\alpha - \lambda_2 D_{\theta+180}^\alpha)$.

The function g is computed for each point on the evolving contour and defined as the difference between the α-th fractional derivative in the normal direction and the α-th order fractional derivative in the opposite direction. The one-sided derivatives are computed using the Eqns. (1, 2).

The idea behind the formulation is that the fractional derivative difference has better capability to capture edges than the integer order derivative-based models which are inherently sensitive to noise. And such a fractional derivative difference attains its maximum value at the object boundary. Once this is incorporated into an evolution equation the active contour reaches out to object boundary efficiently.

Taking the Euler-Lagrange of the energy mentioned above, we have

$$\nabla E^{EDGE} = (\nabla \cdot (\delta g_{\phi_x}, \delta g_{\phi_y}) - g\delta_\phi)|\nabla\phi| + (g_{\phi_x}, g_{\phi_y}) \cdot \nabla(|\nabla\phi|) + \nabla(g\delta) \cdot \vec{N} + g\kappa \qquad (16)$$

with initial condition $\phi(x, y, 0) = \phi_0(x, y)$ on Ω.

2) Balloon Term:

From our understanding of the edge term, we devised a novel bi-directional balloon term as:

$$\nabla E^{NBD} = (-g\delta(\phi))|\nabla\phi| \qquad (17)$$

where $g(x, y) = -(\lambda_1 D_\theta^\alpha - \lambda_2 D_{\theta+180}^\alpha)$. This term entails a normal velocity of magnitude equal to that of the value of g at that contour pixel. The function g incorporated in a traditional balloon term also adaptively directs the curve towards the object boundary faster than the edge term.

B. Evolution Equation

Now we discuss the evolution equation of the proposed model. We combine the terms corresponding to the region scalable data fitting term, the edge term and the balloon term. As discussed above, the balloon and edge term combination evolves the contour to a clear segmentation in presence of high noise. The region scalability brings in a degree of inhomogeneity invariance. So, the proposed model is given as:

$$\begin{aligned}
\frac{\partial \phi}{\partial t} =& \nabla E^{RSF} + \nabla E^{EDGE} + \nabla E^{NBD} \\
=& (-\delta(\phi)(\lambda_1 e_1 - \lambda_2 e_2) + \nu\delta(\phi)div(\frac{\nabla\phi}{|\nabla\phi|})) \\
& + \mu_1((\nabla \cdot (\delta g_{\phi_x}, \delta g_{\phi_y}) - g\delta_\phi)|\nabla\phi| + (g_{\phi_x}, g_{\phi_y}) \cdot \nabla(|\nabla\phi|) \\
& + \nabla(g\delta) \cdot \vec{N} + g\kappa) + \mu_2(-g\delta(\phi)|\nabla\phi|)
\end{aligned}$$
$$(18)$$

In the areas, where the intensity is flat, the response of the fractional derivative-based balloon as well as edge energy terms is reduced. Even though the length of the fractional derivatives in both directions ensures that the contour evolution is sensitive to object contours far away, it is still helpful if the evolution happens under a minimal constant length term alongside the data fitting. Hence, in our equation we have used the length term to speed up contour shrinkage in flat intensity areas.

Also as the algorithm iterations progress, the level set evolves irregularly resulting in steep gradients evolving at some points. As the level set deviates more from the distance function, the computational instability increases. We use the method proposed by Sussman *et al.* [23] to reinitialize the level set back to the distance function in between the iterations. In our algorithm, we re-distance the level set after every iteration. Since the iteration result is reinitialized to steady state of another evolution process, this approach discourages contours evolving in new places.

IV. NUMERICAL IMPLEMENTATION

The computations in region scalable fitting terms involve the convolutions discussed in Eqn. 8 and Eqn. 9 which are handled as mentioned in [11]. The hyperbolic terms in Eqn. 18 are implemented using the entropy conserving methods. Central difference scheme is used for the rest of the terms.

A. Initialization

Active contour methods are sensitive to initialization. Hence various works in literature discuss the performance of their algorithm with respect to a variety of initializations - initializations that overlap with the object, initializations far from object, initial contours of varied shapes and sizes etc. Here we choose an initialization as follows:

$$\phi_0(x,y) = \begin{cases} c_0, & \text{if } 5 \leq x \leq M \text{ and } 5 \leq y \leq N \\ -c_0, & \text{otherwise} \end{cases}$$

Here $\phi_0(x,y)$ is the initial level set function, x and y are image co-ordinates, c_0 is a positive constant value. This initialization is independent of the prior knowledge of the object location.

B. Segmentation Evaluation Metrics

We use Sorenson-Dice and Jaccard coefficients to compare the segmented region and the ground truth. Let P and G denote the prediction and the ground truth respectively. Let $|X|$ denote the cardinality of the set X. Then the Sorenson-Dice coefficient is obtained as:

$$Dice(P,G) = \frac{2 * |P \cap G|}{|P| + |G|} \tag{19}$$

The Jaccard coefficient is obtained as follows:

$$Jaccard(P,G) = \frac{|P \cap G|}{|P \cup G|} \tag{20}$$

In our experiments, the level set region demarcation obtained after convergence is taken as the prediction P. The ground truth G is taken from the source image data sets.

We also compare the boundary detection accuracy under the heavy noise scenario. The precision, recall and the F1 statistical measures are considered for this purpose. Precision denotes the ratio between the number of correctly predicted boundary points and the total number of predicted boundary points. Recall is the ratio between the number of ground truth boundary points that are close within a threshold to the predicted boundary and the total number of the ground truth boundary pixels. In our case, we set the threshold of consideration to 2 pixels keeping in view the boundary distortion due to the high noise incorporated. Given the precision and recall, the F1 score of the boundary is computed as follows:

$$F1(P,G) = \frac{2 * Precision(P,G) * Recall(P,G)}{Precision(P,G) + Recall(P,G)} \tag{21}$$

Our algorithm script is implemented in MATLAB and the functions dice(P,G) and jaccard(P,G) and bfscore(P,G) provide the segmentation accuracy metrics discussed above. The metrics discussed above provide the evaluation of accuracy as a score in the interval [0,1]. This is converted to a percentage and listed in the tables for comparison.

C. Convergence Criterion

In our algorithm, the evolution is stopped when the area inside the curve is no longer changing appreciably as per a fixed threshold. The area difference between segmentation results of two consecutive iterations is estimated as follows in the level set formulation:

$$\Delta Area = |Heaviside(\phi^n > 0) - Heaviside(\phi^{n-1} > 0)| \tag{22}$$

When this $\Delta Area$ is less than 5 units, we stop the iterative process.

V. EXPERIMENTAL RESULTS AND DISCUSSION

Now we demonstrate the working of the proposed model on images with challenging amounts of noise. We have chosen test images from [25] and [24]. We compare the performance of our method against that of the following state-of-the-art methods: a) region scalable fitting (RSF) by Li *et al.* [11] b) locally statistical active contour model (LSACM) by Zhang *et al.* [26] and c) an adaptive fractional order differentiation-based active contour model (AFACM) by Meng Li *et al.* [27].

In each figure panel, the columns are ordered left to right as follows: 1) image with ground truth marked 2) proposed method 3) RSF method 4) LSACM method 5) Adaptive fractional order differentiation method. The rows are ordered top to bottom as follows: 1) original image segmentation 2)image corrupted by Gaussian noise of 0 mean and 0.01 variance 3) image corrupted by Gaussian noise of 0 mean and 0.05 variance 4) image corrupted by multiplicative speckle noise of 0.1 variance 5) image corrupted by salt and pepper noise of density 0.1. MATLAB command *imnoise()* is used for the above mentioned noise addition.

The row-column labels in the tables are self explanatory. For a particular image, the default parameters used for a particular method are mentioned in the respective experiment discussion. Any change in these default parameters for a particular noise are mentioned in the corresponding table in the last column.
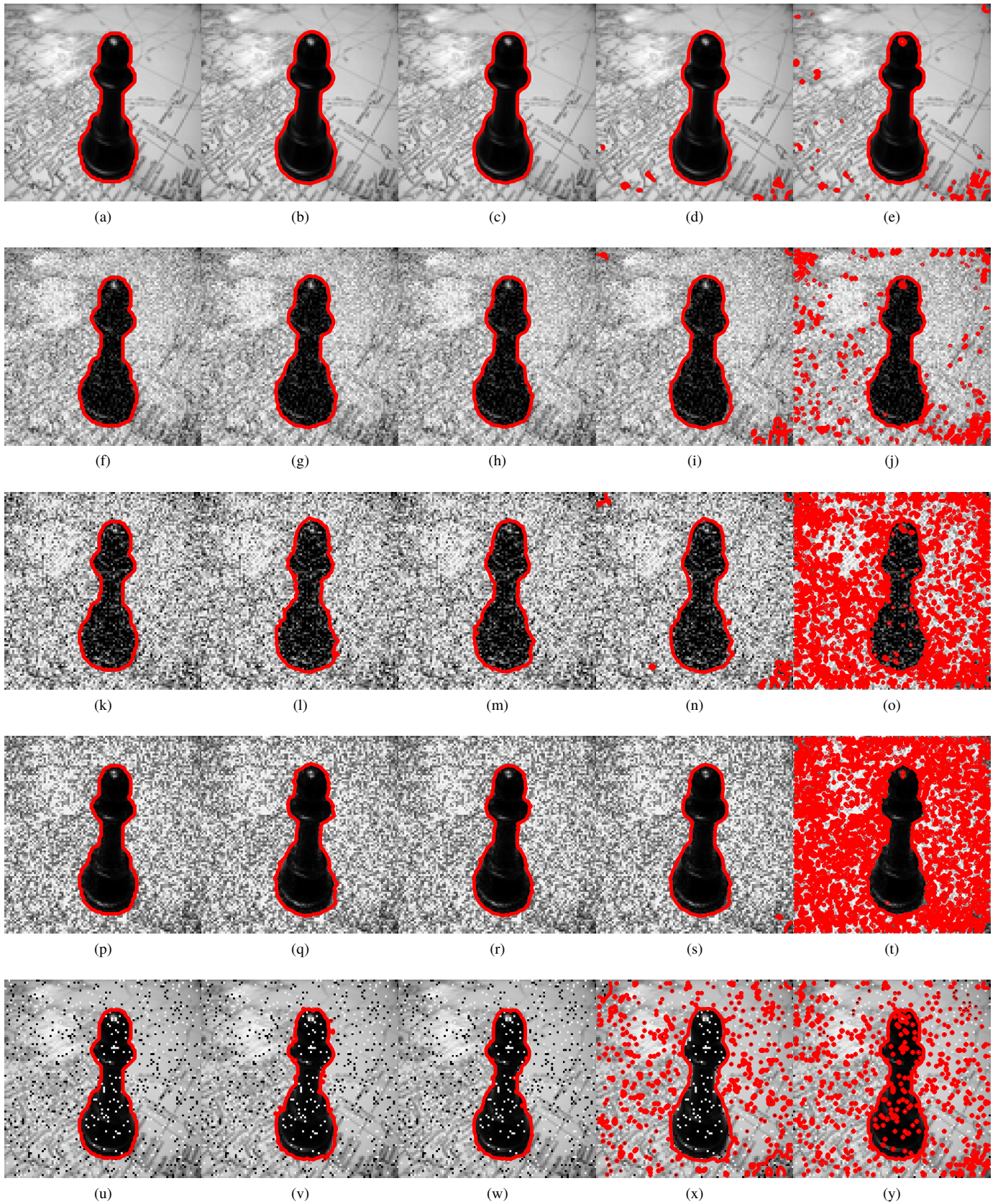
Figure 1: Segmentation on a pawn piece image with distracting edge content

Pawn Image (Fig. 1a)	Dice	Jaccard	Precision	Recall	BF1	Parameters
Proposed method (Fig. 1b)	0.9708	0.9433	0.9711	0.9824	0.9767	
RSF (Fig. 1c)	**0.9874**	**0.9752**	**1**	**1**	**1**	$\sigma = 15$
LSACM (Fig. 1d)	0.9411	0.8888	0.7333	0.9588	0.8311	$\sigma = 7$
AFACM (Fig. 1e)	0.9443	0.8945	0.5945	1	0.7457	$\sigma = 25$
Gaussian Noise (mean=0; var=0.01) (Fig. 1f)	Dice	Jaccard	Precision	Recall	BF1	Parameters
Proposed method (Fig. 1g)	0.9672	0.9365	0.9548	0.9824	0.9684	
RSF (Fig. 1h)	**0.9833**	**0.9671**	**1**	**1**	**1**	$\sigma = 15$
LSACM (Fig. 1i)	0.9257	0.8618	0.6174	0.9412	0.7457	$\sigma = 25$
AFACM (Fig. 1j)	0.8510	0.7406	0.2919	0.9941	0.4513	$\sigma = 25$
Gaussian noise (mean=0; var=0.05) Fig. (1k)	Dice	Jaccard	Precision	Recall	BF1	Parameters
Proposed method (Fig. 1l)	0.9566	0.9168	0.8842	0.9235	0.9034	
RSF (Fig. 1m)	**0.9699**	**0.9416**	**0.9286**	**0.9529**	**0.9406**	$\sigma = 15$
LSACM (Fig. 1n)	0.9136	0.8410	0.5483	0.9059	0.6831	$\sigma = 25$
AFACM (Fig. 1o)	0.5513	0.3806	0.0809	0.9706	0.1493	$\sigma = 25$
Speckle noise (var=0.1) Fig. (1p)	Dice	Jaccard	Precision	Recall	BF1	Parameters
Proposed method (Fig. 1q)	0.9599	0.9230	0.8944	0.9353	0.9144	
RSF (Fig. 1r)	**0.9809**	**0.9625**	**0.9943**	**0.9941**	**0.9942**	$\sigma = 15$
LSACM (Fig. 1s)	0.9616	0.9260	0.8756	0.9647	0.9180	$\sigma = 25$
AFACM (Fig. 1t)	0.4921	0.3263	0.0558	0.9118	0.1051	$\sigma = 25$
Salt and Pepper noise (density=0.1) Fig. (1u)	Dice	Jaccard	Precision	Recall	BF1	Parameters
Proposed (Fig. 1v)	0.9624	0.9276	0.8705	0.9412	0.9044	
RSF (Fig. 1w)	**0.9815**	**0.9637**	**0.9471**	**0.9882**	**0.9672**	$\sigma = 15$
LSACM (Fig. 1x)	0.7571	0.6091	0.1819	0.7882	0.2956	$\sigma = 25$
AFACM (Fig. 1y)	0.7953	0.6602	0.2021	0.9941	0.3358	$\sigma = 25$

Table 1: SEGMENTATION EVALUATION

In the first experiment, we evaluate the segmentation accuracy of the algorithms on the pawn image. As can be seen in Fig. 1a, this image has a lot of edge content in the background of a pawn piece, which can act as distractor for an edge-predominant method like ours. The default parameters are listed below:

Proposed method: $\lambda_1 = \lambda_2 = 0.015, \sigma = 5$, $\nu = 100$, $\mu_1 = 0.1$, $\mu_2 = 0.15$, $\alpha = 0.1$, $\lambda = 10$, $N_1 = N_2 = 100$, $\Delta t = 0.01$

RSF: $\lambda_1 = \lambda_2 = 1$, $\mu = 1, \nu = 0.2 * 255 * 255$, $\Delta t = 0.1$

LSACM: $\mu = 0.1$, $\Delta t = 1$

AFACM: $\lambda = 50, \beta = 1, \mu = 0.1$, $\nu = 0.0002 * 255 * 255$, $\Delta t = 0.02$

As evident from the visual comparison of the subfigures Fig. 1a-Fig. 1y in the panel Fig. 1, the performance of the proposed algorithm is on par with the state-of-the-art methods. Even in the presence of high noise, the proposed method is able to delineate the pawn piece with clear segmentation, while some of the other methods give rise to segmentation marred by artifacts. The evaluation of the segmentation is tabulated in Table 1. The scores listed therein confirm the segmentation accuracy close to that of the best result in each case.
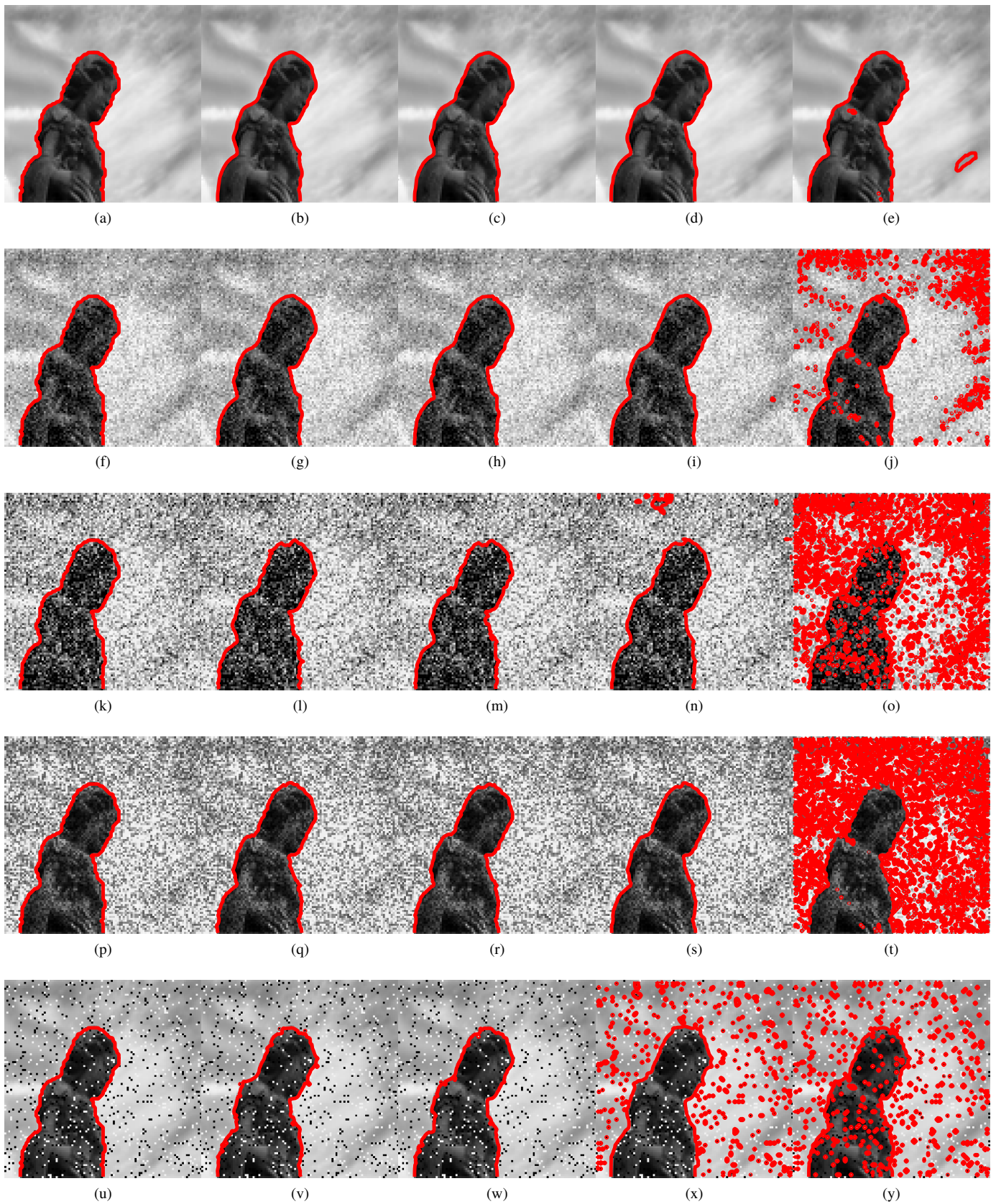
Figure 2: Segmentation on a statue image with uneven illumination

Statue Image(Fig. 2a)	Dice	Jaccard	Precision	Recall	BF1	Parameters
Proposed method (Fig. 2b)	**0.9959**	**0.9918**	1	1	1	
RSF (Fig. 2c)	0.9944	0.9888	1	1	1	$\sigma = 15$
LSACM (Fig. 2d)	0.9944	0.9889	1	1	1	$\sigma = 17$
AFACM (Fig. 2e)	0.9871	0.9746	0.8455	1	0.9163	
Gaussian Noise (mean=0; var=0.01) (Fig. 2f)	Dice	Jaccard	Precision	Recall	BF1	Parameters
Proposed method (Fig.2g)	**0.9933**	**0.9867**	1	1	1	
RSF(2h)	0.9922	0.9845	1	1	1	$\sigma = 25$
LSACM(2i)	0.9931	0.9863	0.9855	1	0.9927	$\sigma = 25$
AFACM(2j)	0.8569	0.7497	0.2188	1	0.3591	
Gaussian noise (mean=0; var=0.05) (Fig.2k)	Dice	Jaccard	Precision	Recall	BF1	Parameters
Proposed method (Fig.2l)	**0.9845**	**0.9696**	**0.9673**	**0.9807**	**0.9739**	
RSF (Fig. 2m)	0.9825	0.9656	0.9393	0.9614	0.9502	$\sigma = 25$
LSACM (Fig. 2n)	0.9741	0.9495	0.7923	0.9903	0.8803	$\sigma = 25$
AFACM (Fig. 2o)	0.6590	0.4915	0.0939	1	0.1717	
Speckle noise (var=0.1) Fig. 2p)	Dice	Jaccard	Precision	Recall	BF1	Parameters
Proposed method (Fig.2q)	**0.9890**	**0.9782**	1	1	1	
RSF (Fig. 2r)	0.9885	0.9773	0.9905	0.9903	0.9904	$\sigma = 25$
LSACM (Fig. 2s)	0.9905	0.9811	0.9952	0.9952	0.9952	$\sigma = 25$
AFACM (Fig. 2t)	0.6205	0.4498	0.0801	1	0.1483	
Salt and Pepper noise (density=0.1) (Fig.2u)	Dice	Jaccard	Precision	Recall	BF1	Parameters
Proposed method (Fig. 2v)	**0.9883**	**0.9769**	**0.9430**	1	**0.9707**	
RSF (Fig. 2w)	0.9845	0.9695	0.9292	0.9855	0.9565	$\sigma = 25$
LSACM (Fig. 2x)	0.9043	0.8254	0.3187	0.9372	0.4757	$\sigma = 25$
AFACM (Fig. 2y)	0.8962	0.8120	0.2613	1	0.4144	

Table 2: Segmentation Evaluation

In the second experiment, we test the algorithms' performance on the image of a statue against the background of sky with wide variation in illumination. The uneven intensities all over the background make the task of segmentation challenging. The default parameters are listed below:

Proposed method: $\lambda_1 = \lambda_2 = 0.01$, $\sigma = 5$, $\nu = 100$, $\mu_1 = 0.1$, $\mu_2 = 0.01$, $\alpha = 0.1$, $\lambda = 10$, $N_1 = N_2 = 100$, $\Delta t = 0.01$

RSF: $\lambda_1 = \lambda_2 = 1$, $\mu = 1$,$\nu = 0.2 * 255 * 255$, $\Delta t = 0.1$
LSACM: $\mu = 0.1$, $\Delta t = 1$

AFACM:$\lambda = 50$,$\beta = 1$,$\mu = 0.1$, $\nu = 0.0002 * 255 * 255$, $\Delta t = 0.02$,$\sigma = 25$

In this case, we find that the proposed method gives a clean segmentation, (Figs. 2b, 2g, 2l, 2q, and 2v)- slightly better than state-of-the-art methods, which generally deal well with intensity inhomogeneity. This can be attributed to the combination of RSF kernel with the fractional derivative-based terms which is effectively segmenting the target object in presence of illumination variance as well as high amounts of noise. The segmentation evaluation scores are tabulated in Table 2.

Figure 3: Segmentation on a towers image with spot illumination effect

Towers image (Fig. 3a)	Dice	Jaccard	Precision	Recall	BF1	Parameters
Proposed method (Fig.3b)	**0.9769**	**0.9548**	**0.9496**	**0.9479**	**0.9488**	
RSF (Fig. 3c)	0.9001	0.8184	0.7422	0.8958	0.8118	$\sigma = 15$
LSACM (Fig. 3d)	0.9022	0.8218	0.7319	0.9107	0.8115	$\sigma = 10$
AFACM (Fig. 3e)	0.8974	0.8183	0.6723	0.9057	0.7717	
Gaussian Noise (mean=0; var=0.01) (Fig. 3f)	Dice	Jaccard	Precision	Recall	BF1	Parameters
Proposed method (Fig.3g)	**0.9747**	**0.9506**	**0.9426**	**0.9504**	**0.9465**	
RSF (Fig. 3h)	0.8929	0.8066	0.6994	0.8610	0.7718	$\sigma = 20$
LSACM (Fig. 3i)	0.8950	0.8099	0.6814	0.8511	0.7568	$\sigma = 25$
AFACM (Fig. 3j)	0.8812	0.7876	0.3217	0.9156	0.4761	
Gaussian noise (mean=0; var=0.05) (Fig. 3k)	Dice	Jaccard	Precision	Recall	BF1	Parameters
Proposed method (Fig.3l)	**0.9678**	**0.9376**	**0.8589**	**0.8958**	**0.8769**	
RSF (Fig. 3m)	0.8801	0.7859	0.6328	0.8139	0.7120	$\sigma = 25$
LSACM (Fig. 3n)	0.8895	0.8009	0.5829	0.8213	0.6819	$\sigma = 25$
AFACM (Fig. 3o)	0.7852	0.6463	0.1637	0.9256	0.2782	
Speckle noise (var=0.1) Fig. 3p)	Dice	Jaccard	Precision	Recall	BF1	Parameters
Proposed method (Fig.3q)	**0.9708**	**0.9432**	**0.9160**	**0.9181**	**0.9171**	
RSF (Fig. 3r)	0.8838	0.7918	0.6454	0.8189	0.7219	$\sigma = 25$
LSACM (Fig. 3s)	0.8924	0.8057	0.5779	0.7717	0.6609	$\sigma = 25$
AFACM (Fig. 3t)	0.7947	0.6594	0.2022	**0.9727**	0.3347	
Salt and Pepper noise (density=0.1) (Fig.3u)	Dice	Jaccard	Precision	Recall	BF1	Parameters
Proposed method (Fig.3v)	**0.9680**	**0.9380**	**0.8568**	**0.9305**	**0.8922**	
RSF (Fig. 3w)	0.8910	0.8034	0.6896	0.8635	0.7668	$\sigma = 25$
LSACM (Fig. 3x)	0.9079	0.8314	0.6297	0.8734	0.7318	$\sigma = 25$
AFACM (Fig. 3y)	0.8481	0.7362	0.2665	0.9330	0.4146	

Table 3: Segmentation Evaluation

In our next experiment, we test the efficacy of proposed algorithm on an image of two towers. This image also has challenging spot illumination due to the presence of sun in the background sky. The spot intensity spiking has the effect of eroding the boundary information of the tower. The presence of clouds further complicates image segmentation. The default parameters are listed below:

Proposed method: $\lambda_1 = \lambda_2 = 0.015$, $\sigma = 5$, $\nu = 100$, $\mu_1 = 0.1$, $\mu_2 = 0.01$, $\alpha = 0.3$, $\lambda = 10$, $N_1 = N_2 = 100$, $\Delta t = 0.01$

RSF: $\lambda_1 = \lambda_2 = 1$, $\mu = 1$, $\nu = 0.2 * 255 * 255$, $\Delta t = 0.1$
LSACM: $\mu = 0.1$, $\Delta t = 1$

AFACM: $\lambda = 50$, $\beta = 1$, $\mu = 0.1$, $\nu = 0.0002 * 255 * 255$, $\Delta t = 0.02$, $\sigma = 25$

In these challenging situations too, the proposed method is able to segment the towers selectively and consistently across the various noises added, as seen in the panel of images shown in Fig. 3. We find that responses of other methods are either affected by noise resulting in artifacts or digressed due the cloud presence, resulting in incorrect segmentation in certain portions of the image. The evaluation scores tabulated in Table 3 again confirm the superior segmentation performance of the proposed method in comparison with other methods.
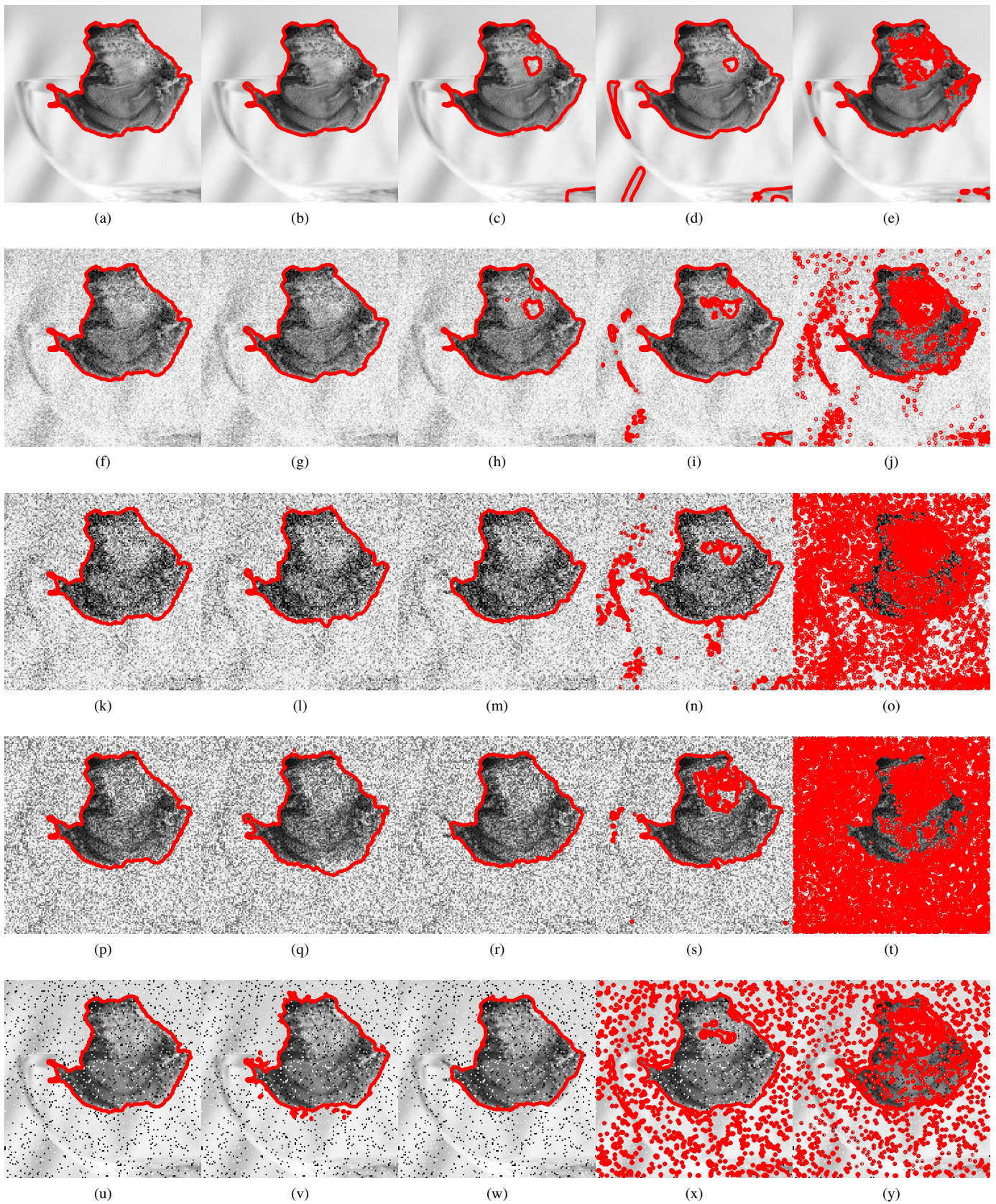
Figure 4: Segmentation on a frog image

Frog image (Fig. 4a)	Dice	Jaccard	Precision	Recall	BF1	Parameters
Proposed method (Fig.4b)	**0.9892**	**0.9786**	**0.9747**	**0.9755**	**0.9751**	
RSF (Fig. 4c)	0.9814	0.9635	0.9055	0.8865	0.8959	$\sigma = 50, \nu = 0.1 * 255 * 255$
LSACM (Fig. 4d)	0.9313	0.8715	0.5198	0.9632	0.6752	
AFACM (Fig. 4e)	0.9097	0.8344	0.3293	0.9110	0.4837	$\lambda = 25, \sigma = 50$
Gaussian noise (mean=0; var=0.01) (Fig. 4f)	Dice	Jaccard	Precision	Recall	BF1	Parameters
Proposed method (Fig.4g)	**0.9853**	**0.9710**	**0.9379**	**0.9540**	**0.9459**	
RSF (Fig. 4h)	0.9758	0.9527	0.8576	0.9049	0.8806	$\sigma = 50, \nu = 0.1 * 255 * 255$
LSACM (Fig. 4i)	0.9409	0.8884	0.4718	0.9448	0.6294	
AFACM (Fig. 4j)	0.8503	0.7395	0.1884	0.9663	0.3153	$\lambda = 25, \sigma = 50$
Gaussian noise (mean=0; var=0.05) (Fig. 4k)	Dice	Jaccard	Precision	Recall	BF1	Parameters
Proposed method (Fig.4l)	**0.9755**	**0.9521**	**0.8736**	0.9325	**0.9021**	
RSF (Fig. 4m)	0.9709	0.9435	0.8678	0.8006	0.8329	$\sigma = 50$
LSACM (Fig. 4n)	0.9162	0.8454	0.3644	0.9264	0.5230	
AFACM (Fig. 4o)	0.6501	0.4816	0.0860	**0.9969**	0.1583	$\lambda = 25, \sigma = 50$
Speckle noise (var=0.1) Fig. 4p)	Dice	Jaccard	Precision	Recall	BF1	Parameters
Proposed method (Fig.4q)	0.9615	0.9259	0.8333	0.8773	**0.8548**	
RSF (Fig. 4r)	**0.9687**	**0.9392**	**0.8448**	0.7730	0.8073	$\sigma = 55$
LSACM (Fig. 4s)	0.9162	0.8453	0.4274	0.8865	0.5767	
AFACM (Fig. 4t)	0.5740	0.4025	0.0661	**0.9969**	0.1239	$\lambda = 50, \sigma = 25$
Salt and pepper noise (density=0.1) Fig.4u)	Dice	Jaccard	Precision	Recall	BF1	Parameters
Proposed method (Fig.4v)	**0.9807**	**0.9621**	0.8299	**0.9724**	**0.8955**	
RSF (Fig. 4w)	0.9722	0.9459	**0.8621**	0.7883	0.8236	$\sigma = 50$
LSACM (Fig. 4x)	0.8651	0.7623	0.1897	0.9479	0.3162	
AFACM (fig. 4y)	0.7922	0.6560	0.1539	0.9233	0.2639	$\lambda = 50, \sigma = 25$

Table 4: Segmentation Evaluation

In the fourth experiment, we show the segmentation result on the image showing a frog on glassware. In this case, the image is rife with several patterns which may be incorrectly delineated by the methods as the boundary of the frog's body. Further challenge is to find the body contour of the frog under various noises. The default parameters are listed below:

Proposed method: $\lambda_1 = \lambda_2 = 0.025$, $\sigma = 5$, $\nu = 100$, $\mu_1 = 0.1$, $\mu_2 = 0.1$, $\alpha = 0.1$, $\lambda = 10$, $N_1 = N_2 = 100$, $\Delta t = 0.01$

RSF: $\lambda_1 = \lambda_2 = 1$, $\mu = 1$, $\nu = 0.2 * 255 * 255$, $\Delta t = 0.1$

LSACM: $\sigma = 25$, $\mu = 0.1$, $\Delta t = 1$

AFACM: $\beta = 1$, $\mu = 0.1$, $\nu = 0.0002 * 255 * 255$, $\Delta t = 0.02$,

Here too we find the proposed method is able to segment the target effectively as shown in the image panel Fig. 4. The quantitative evaluation scores for this image are tabulated in Table 4.
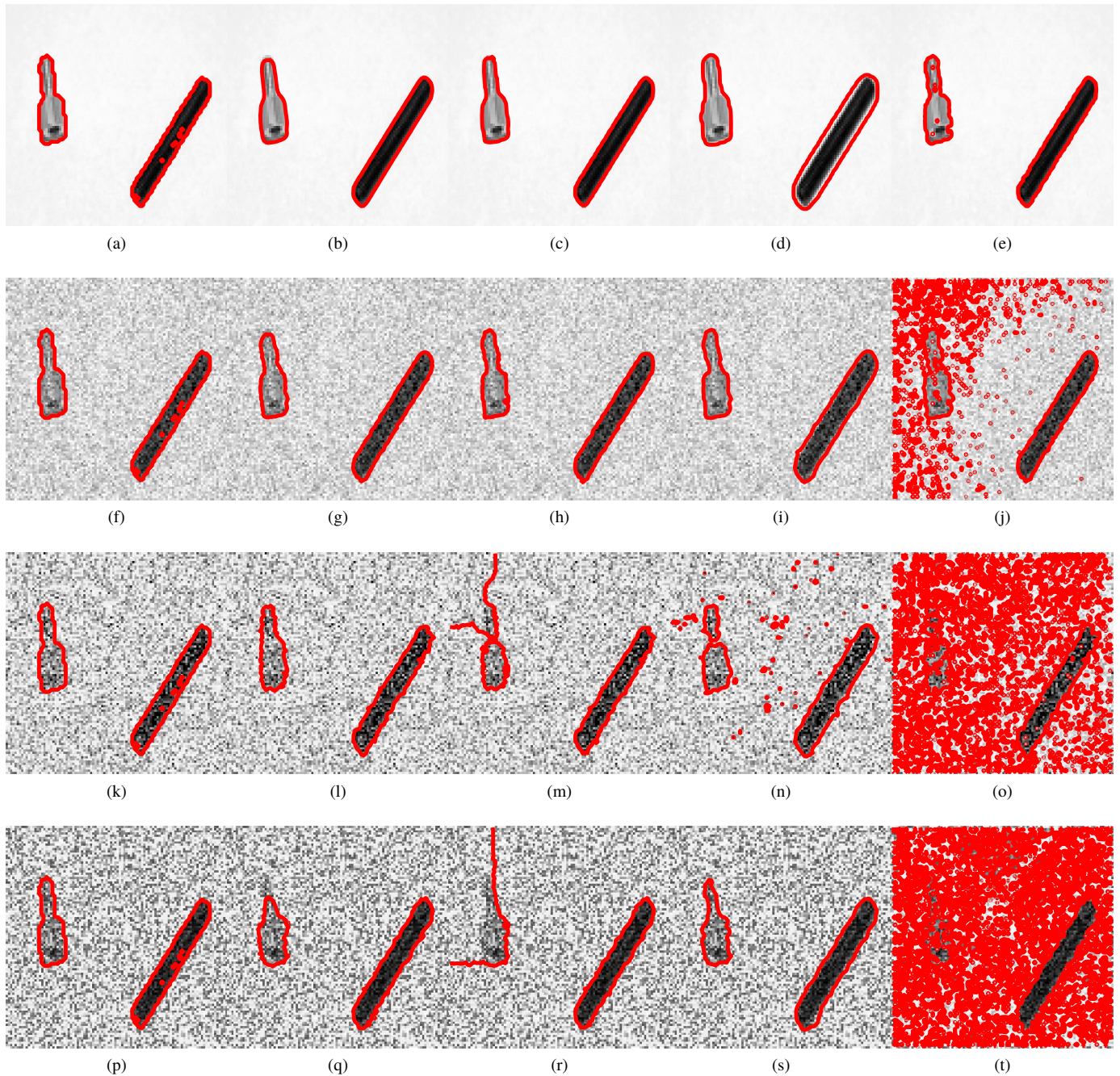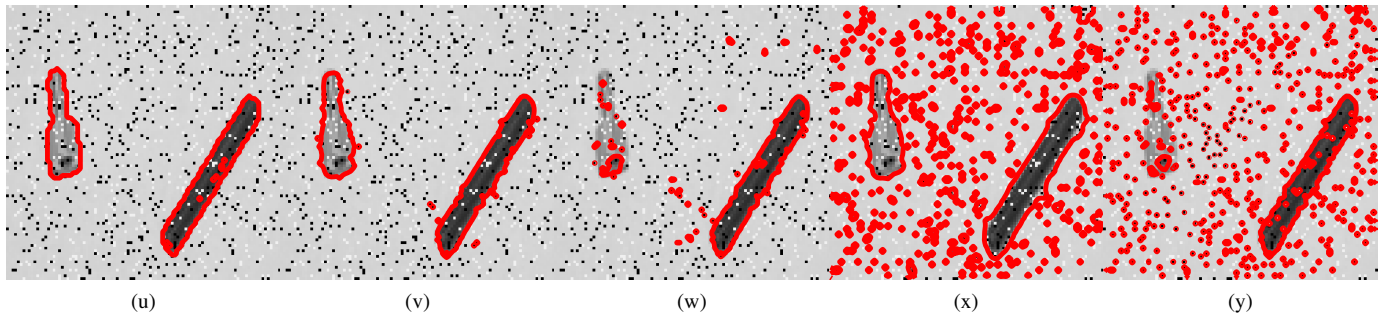

Figure 5: Segmentation on a key and a pen image

Figure 5: Segmentation on a key and a pen image

In the last experiment, we show the segmentation evaluation on an image having a pen and key. Seemingly simple, this image has the key, the pen and the background - all having different intensities. In presence of noise , the objects are not easy to distinguish especially the boundary of the key. The default parameters are listed below:

Proposed method: $\lambda_1 = \lambda_2 = 0.015$, $\sigma = 5$, $\nu = 100$, $\mu_1 = 0.015$, $\mu_2 = 0.01$, $\alpha = 0.3$, $\lambda = 10$, $N_1 = N_2 = 100$, $\Delta t = 0.01$

RSF: $\lambda_1 = \lambda_2 = 1$, $\mu = 1$, $\nu = 0.1 * 255 * 255$, $\Delta t = 0.1$, $\sigma = 15$

LSACM: $\mu = 0.1$, $\Delta t = 1$

AFACM: $\beta = 1$, $\mu = 0.1$, $\nu = 0.0002 * 255 * 255$, $\Delta t = 0.02$, $\sigma = 15$

Here also we can observe that the proposed method is able to segment the boundaries stably as seen in Fig. 5. The segmentation evaluation scores for this image are tabulated in Table 5.

Key and a pen image (Fig. 5a)	Dice	Jaccard	Precision	Recall	BF1	Parameters
Proposed method (Fig.5b)	0.9634	0.9294	0.9949	0.9027	0.9466	
RSF (Fig. 5c)	**0.9686**	**0.9391**	**1**	**0.9115**	**0.9537**	$\sigma = 10$
LSACM (Fig. 5d)	0.8387	0.7222	0.4953	0.4469	0.4699	$\sigma = 10$
AFACM (Fig. 5e)	0.9645	0.9315	0.9196	0.9071	0.9133	
Gaussian noise (mean=0; var=0.01) (Fig. 5f)	Dice	Jaccard	Precision	Recall	BF1	Parameters
Proposed method (Fig.5g)	0.9595	0.9221	0.9950	0.8982	0.9442	
RSF (Fig. 5h)	**0.9651**	**0.9326**	**0.9952**	**0.9115**	**0.9515**	
LSACM (Fig. 5i)	0.9074	0.8304	0.8852	0.7920	0.8360	$\sigma = 10$
AFACM (Fig. 5j)	0.6082	0.4370	0.1951	0.9115	0.3214	
Gaussian noise (mean=0; var=0.05) (Fig. 5k)	Dice	Jaccard	Precision	Recall	BF1	Parameters
Proposed method (Fig.5l)	**0.9283**	**0.8661**	**0.9269**	0.8584	**0.8914**	
RSF (Fig. 5m)	0.6688	0.5024	0.6405	0.8186	0.7187	
LSACM (Fig. 5n)	0.8559	0.7481	0.6154	0.7743	0.6858	$\sigma = 15$
AFACM (Fig. 5o)	0.3381	0.2035	0.0895	**0.9204**	0.1631	

Speckle noise (var=0.1) Fig. 5p)	Dice	Jaccard	Precision	Recall	BF1	Parameters
Proposed method (Fig.5q)	**0.8965**	**0.8124**	**0.9034**	0.7965	**0.8466**	
RSF (Fig. 5r)	0.5755	0.4040	0.5733	0.7257	0.6406	
LSACM (Fig. 5s)	0.8882	0.7990	0.8744	0.7920	0.8312	$\sigma = 15$
AFACM (Fig. 5t)	0.2878	0.1681	0.0678	**0.8673**	0.1258	
Salt and pepper noise (density=0.1) Fig.5u)	Dice	Jaccard	Precision	Recall	BF1	Parameters
Proposed method (Fig.5v)	**0.9333**	**0.8749**	**0.9079**	**0.8938**	**0.9008**	
RSF (Fig. 5w)	0.7346	0.5805	0.7095	0.6549	0.6811	
LSACM (Fig. 5x)	0.6636	0.4966	0.2076	0.7566	0.3258	$\sigma = 15$
AFACM (fig. 5y)	0.5582	0.3871	0.2401	0.7124	0.3592	

Table 5: SEGMENTATION EVALUATION

As can be seen from the parameters listing for all the methods, the proposed method parameters are the same for all tests for a particular image - noiseless as well as noisy scenarios. For other methods, the value of scale parameter has to be increased often to cope with the noise. But in our case, we keep the scale parameter fixed at $\sigma = 5$ in all experiments. In proposed method, the set of parameter values (the coefficients for rsf, balloon and edge terms) once selected for a particular image, provide a top quality segmentation even if high noise were to be added to the given image.

VI.   CONCLUSION

This paper presents a novel combination of a fractional derivative-based balloon term, a fractional derivative edge term and region scalable fitting term for efficient segmentation. Image border initialization has been used which makes the segmentation independent of the prior knowledge of the object location. It was also shown that in case of the proposed method, the same set of method parameters that provide best segmentation in noiseless scenario provide an equally good segmentation in high noise scenarios. By testing on challenging natural images in presence of high noise levels, the method has been demonstrated to be efficient in delineating the object boundaries.

ACKNOWLEDGMENTS

REFERENCES

[1] M. Kass, A. Witkin, D. Terzopoulos, Snakes: Active contour models, International Journal of Computer Vision, 1(4) (1988) 321-331.

[2] S. Osher, J. A. Sethian, Fronts propagating with curvature-dependent speed: Algorithms based on Hamilton-Jacobi formulations, Journal of Computational Physics, 79(1) (1988) 12-49.

[3] V. Caselles, R. Kimmel, and G. Sapiro, Geodesic Active Contours, International Journal of Computer Vision, 22(1) (1997) 61-79.

[4] S. Kichenassamy, A. Kumar, P. Oliver, A. Tannenbaum and A. Yezzi, Gradient flows and geometric active contour models, Proceedings of 5th International Conference on Computer Vision, (1995) 810-815.

[5] C. Li, C. Xu, C. Gui and M. D. Fox, Level set evolution without re-initialization: A new variational formulation, Proceedings of IEEE Conference on Computer Vision and Pattern Recognition, 1 (2005) 430-436.

[6] C. Li, C. Xu, C. Gui and M. D. Fox, Distance Regularized Level Set Evolution and Its Application to Image Segmentation, IEEE Transactions on Image Processing, 19(12) (2010) 3243-3254.

[7] D. Mumford, J. Shah, Optimal approximations by piecewise smooth functions and associated variational problems, Communications on Pure and Applied Mathematics, 42(5) (1989) 577-685.

[8] T. F. Chan and L. A. Vese, Active contours without edges, IEEE Transactions on Image Processing, 10(2) (2001) 266-277.

[9] A. Yezzi, A. Tsai and A. Willsky, A statistical approach to snakes for bimodal and trimodal imagery, Proceedings of International Conference on Computer Vision, 2 (1999) 898-903.

[10] D. Cremers, M. Rousson and R. Deriche, A review of statistical approaches to level set segmentation: Integrating color, texture, motion, and shape, International Journal of Computer Vision, 72(2) (2007) 195-215.

[11] C. Li, C. Kao, J. C. Gore and Z. Ding, Minimization of Region-Scalable Fitting Energy for Image Segmentation, IEEE Transactions on Image Processing, 17(10) (2008) 1940-1949.

[12] S. Lankton, A. Tannenbaum, Localizing region-based active contours, IEEE Transactions in Image Processing, 17(11) (2008) 2029-2039.

[13] W. Kim and C. Kim, Active Contours Driven by the Salient Edge Energy Model, IEEE Transactions on Image Processing, 22(4) (2013) 1667-1673.

[14] A. Khadidos, V. Sanchez and C. Li, Weighted Level Set Evolution Based on Local Edge Features for Medical Image Segmentation, IEEE Transactions on Image Processing, 26(4) (2017) 1979-1991.

[15] Z. Ren, Variational level set method for two-stage image segmentation based on morphological gradients, Mathematical Problems in Engineering, 2014 (2014) 1-11 .

[16] H. Liv, F. Zhang, and R. Wang, Fuzzy active contour model using fractional-order diffusion based edge indicator and fuzzy local fitted image, IEEE Access, 8 (2020) 172707-172722.

[17] Al-Shamasneh A.R., Jalab H.A., Alkahtani H., Edge Based Method for Kidney Segmentation in MRI Scans, Advances and Trends in Artificial Intelligence - From Theory to Practice, IEA/AIE 2021, Springer Lecture Notes in Computer Science, 12799 (2021).

[18] M. Li, Y. Zhan, and Y. Ge, Fractional distance regularized level set evolution with its application to image segmentation, IEEE Access, 8 (2020) 84604-84617.

[19] M. Gu and R. Fang Wang, Fractional differentiation-based active contour model driven by local intensity fitting energy, Mathematical Problems in Engineering, 2016 (2016) 1-10.

[20] Z. Ren, Adaptive active contour model driven by fractional-order fitting energy, Signal Processing, 117 (2015) 138-150.

[21] B. Chen, S. Huang, Z. Liang, W. Chen, and B. Pan, A fractional order derivative based active contour model for inhomogeneous image segmentation, Applied Mathematical Modelling, 65 (2019) 120-136.

[22] S. Khanna, V. Chandrasekaran, Fractional Differentiation-Based Edge Energy Driven Active Contours for Robust Image Segmentation, ICTACT Journal of Image and Video Processing, August (2021).

[23] Sussman, M., Smereka, P. and Osher, S. J., A level set approach for computing solutions to incompressible two phase flow, Journal of Computational Physics, 114 (1994) 146-159.

[24] Ming-Ming Cheng, Niloy J. Mitra, Xiaolei Huang, Philip H. S. Torr and Shi-Min Hu, Global Contrast based Salient Region Detection, IEEE Transactions in Pattern Analysis and Machine Intelligence, 37(3) (2015) 569-582.

[25] Sharon Alpert, Meirav Galun, Ronen Basri and Achi Brandt, Image Segmentation by Probabilistic Bottom-Up Aggregation and Cue Integration, Proceedings of the IEEE Conference on Computer Vision and Pattern Recognition, June (2007).

[26] K. Zhang, L. Zhang, K. Lam and D. Zhang, A Level Set Approach to Image Segmentation With Intensity Inhomogeneity, IEEE Transactions on Cybernetics, 46(2) (2016) 546-557.

[27] M. M. Li and B. Z. Li, A Novel Active Contour Model for Noisy Image Segmentation Based on Adaptive Fractional Order Differentiation, IEEE Transactions on Image Processing, 29 (2020) 9520-9531.